lative to that of the bulk TiO_2. This shift indicates that the TiO_2 particles inside ZSM-5 framework are extremely small and size-dependent.

It was interested to note that two types of TiO_2 species are present, as demonstrated by UV-VIS spectroscopy. This phenomena may tentatively be explained as follows. The onset of *ca.* 325 nm might be attributed to the formation of nanoscale TiO_2 clusters inside the zeolite cavities formed by channel intersections. The second type of the TiO_2 particles may be involved with the onset of *ca.* 380 nm, which might be rod-like particles grown inside the zeolite channels. The formation of analogous particles has been reported earlier for the zeolites with different channel structure, *viz* mordenite and L zeolite.[4]

Conclusions

1. The procedure developed for the TiO_2 deposition on ZSM-5 zeolite does not cause any marked damage of the zeolite structure.

2. The TiO_2 paticles embedded are uniformly distributed inside the zeolite framework without localization onto the zeolite external surfaces.

3. The TiO_2 particles thus embedded appear to be small enough to exhibit the properties typical of quantum-sized particles.

References

1. (a) Stucky, G. D.; Mac Dougall, J. E. *Science* **1990**, *247*, 669. (b) Ozin, G. A. *Adv. Mater.* **1992**, *4*, 612. *Stud. in Surf. Sci. & Catal.* **1997**, *105*, 1077.
2. Komaya, T.; Bell, A. T.; Weng-Sieh, Z.; Gronsky, R.; Engelke, F.; King, T. S.; Pruski, M. *J. Catal.* **1994**, *150*, 400.
3. Klaas, J.; Kulawik, K.; Schulz-Ekloff, G.; Jaeger, N. I. *Stud. Surf. Sci. Catal.* **1994**, *84*, 2261.
4. Liu, X.; Iu, K.-K.; Thomas, J. K. *J. Chem. Soc., Faraday Trans.* **1993**, *89*, 1861.
5. Haukka, S.; Lakomaa, E.-L.; Root, A. *J. Phys. Chem.* **1993**, *97*, 5085.
6. Blasco, T.; Camblor, M. A.; Perez-Pariente, J. *J. Am. Chem. Soc.* **1993**, *115*, 11806.
7. (a) Brus, L. E. *J. Chem. Phys.* **1983**, *79*, 5566. (b) Henglein, A. *Chem. Rev.* **1989**, *89*, 1861.

Microstructure, Electrical Property and Nonstoichiometry of Light Enhanced Plating (LEP) Ferrite Film

Don Kim*, Choong Sub Lee†, and Yeong Il Kim

Department of Chemistry, †Department of Physics,
Pukyong National University, Pusan 608-737, Korea
Received November 15, 1997

A magnetic film was deposited on a slide glass substrate from aqueous solutions of $FeCl_2$ and $NaNO_2$ at 363 K. XRD analysis showed that the film was polycrystalline magnetite ($Fe_{3(1-\delta)}O_4$) without impurity phase. The lattice constant was 0.8390 nm. Mössbauer spectrum of the film could be deconvoluted by the following parameters: isomer shifts for tetrahedral (T_d) and octahedral (O_h) sites are 0.28 and 0.68 mm/s, respectively, and corresponding magnetic hyperfine fields are 490 and 458 kOe, respectively. The estimated chemical formula of the film by the peak intensity of Mössbauer spectrum was $Fe_{2.95}O_4$. Low temperature transition of the magnetite (Verwey transition) was not detected in resistivity measurement of the film. Properties of the film were discussed with those of pressed pellet and single crystal of synthetic magnetites. On the surface of the film, magnetite particles of about 0.2 μm in diameter were identified by noncontact atomic force microscopy (NAFM) and magnetic force microscopy (MFM).

Introduction

Thin liquid film plating technique invented by Abe *et al.*[1] is a very useful method to synthesize magnetite thin films from aqueous solution at low temperature, especially below 100 °C.[1] They found that light irradiation during the plating process (Light Enhanced Plating: LEP) increases the film deposition rate due to the local heating effect.[2] LEP technique has many advantages: high deposition rate (~0.3 μm/min),[2,3] easy doping of foreign atoms ($Fe_{3-x}M_xO_4$; M=transition metal),[3] and mass production of films.[1] And various materials (glass, quartz, semiconductors and most of polymers) could be used as a substrate for LEP technique.[3] The ferrite films prepared by this method are strongly compatible with water and some organic compounds due to hydrophilic nature of ferrite film structure.[4] Therefore, the ferrite films have many potential applications from bio-sensors to electronic devices.[5-7]

Many works have been reported for the surface of magnetites since scanning probe microscope (SPM) was invented.[8] For example, Wiesendanger *et al.* reported[9] ord-

ering of Fe^{3+} and Fe^{2+} ions on (001) surface of natural magnetite. Molony *et al.* reported[10] various magnetic domain structures below Verwey transition temperature of synthetic magnetite with MFM. Yuan *et al.* reported[11] AFM image of submicron scale particles of magnetite powder. MFM is a relatively new technique and very helpful tool to understand micromagnetic structure of surface of LEP film.[10] However, submicro-structure and submicromagnetic information for the LEP film have not been reported by this time. Therefore we studied submicro-structure of the LEP film with MFM and NAFM.

Physical properties of magnetite greatly depend on the nonstoichiometric value (δ) of $Fe_{3(1-\delta)}O_4$. Tamaura *et al.* reported relationship between lattice parameter (a_o) and δ of magnetite powder.[12] According to their report, the lattice parameter (a_o) of $Fe_{3(1-\delta)}O_4$ decreased when δ increased: a_o= 0.8418 nm for $3\delta = -0.127$, a_o=0.83967 nm for 3δ=0.000, a_o =0.8394 nm for 3δ=0.017, a_o=0.8389 nm for 3δ=0.113.[12] Alekseyeva also found similar result with electrochemically modified magnetite crystal.[13] Honig *et al.* have reported that Verwey transition temperature (Tv) depends linearly on the amount of δ or transition metal impurities ($Fe_{3-x}M_xO_4$; $x=3\delta$) from the measurement of several physical properties:[14-19] Tv =~121 K for 3δ=0, ~83 K for 3δ=0.039, and no transition for $3\delta > 0.039$. Recent electrical resistivity studies showed that when a magnetite sample has different stoichiometric phases, Tv of the sample corresponds to that of more stoichiometric phase.[17] Therefore if Verwey transition of a sample appeared in the temperature range of 83 K-121 K, it is possible to estimate δ of the magnetite phase.[20]

It is very hard to determine the exact value of δ in $Fe_{3(1-\delta)}O_4$ with small amount of magnetite which is deposited on a substrate. As far as we know, there is no report where exact δ value of a magnetite film was determined[21-24] except Abe's group[25] who adopted standard colorimetric method utilizing 2,2'-bipyridyl complex[26] to determine δ. We have found that this method needs very careful procedure to avoid air oxidation and enough amount of ferrite (~20 mg) to get a reasonable data. But the method gave reasonable value for the total amount of iron in the film. Instead of determining δ, therefore, this method was used to estimate thickness of LEP film with density of magnetite. Mössbauer spectroscopy is another method to determine the nonstoichiometry of magnetite.[27-29] This method is imprecise to determine a small deviation from ideal ratio but suffice to estimate the large differences in site population of iron ions between stoichiometric and nonstoichiometric magnetites.[27]

This work reports the first study of submicromagnetic structure of LEP film by using MFM/NAFM at room temperature. We estimate nonstoichiometry of LEP film by Mössbauer spectroscopy and XRD, and suggest the cation distributions in the film and pressed magnetite with resistivity measurement and δ *vs.* Tv relationship of magnetite. Properties of LEP film were discussed comparatively with those of pressed pellets and single crystal of synthetic magnetites.

Experiments

Film synthesis. Figure 1 shows homemade instrumentation for the LEP technique. We slightly modified that

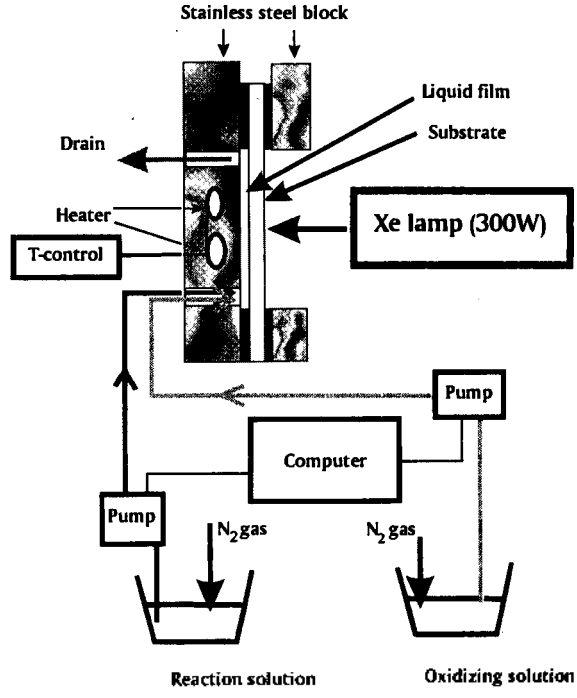

Figure 1. Schematic diagram of the Light Enhanced ferrite Plating (LEP).

of Abe *et al.*[1] Followings are short descriptions of the set-up and best deposition condition. While the reaction solution flowed through the gap between slide glass substrate and stainless steel block 300 W white light from Xe-lamp (Ataco XC300) was focused in 1 cm diameter on the other side of the substrate. The film was deposited on a substrate between the gap. Flow rates of reaction ($FeCl_2$, 6 mL/min) and oxidant ($NaNO_2$, 11 mL/min) solutions were controlled by two LC-pumps (Pharmacia Biotech P-50). The reaction solution and the oxidant solution were alternately pumped for 5 sec and 0.5 sec, respectively. Flow time was controlled by a personal computer and an interface board (Metrabyte DAS1602). Both solutions were buffered to pH 6.3 by addition of CH_3COONH_4 (Aldrich 99%, 5 g/L). Concentrations of $FeCl_2$ (Aldrich 99%) and $NaNO_2$ (Aldrich 99%) were 3.0 g/L and 1.0 g/L, respectively. All solutions were purged with nitrogen gas (Daesung 99.99%) before the reaction for 2 hrs and during the reaction continuously. The reaction temperature was controlled to 363 K by a temperature controller (Hanyoung DX7) and two cartridge heaters (Kwangmyung 45 W). Total deposition time was 20 min. Thickness (~3.5 μm) of the film was estimated from film area and total Fe concentration which was determined by the colorimetric method[25] assuming that LEP film had ideal density of magnetite (5.2 g/cm^3).

Characterization of the LEP film. Surface morphology of the film was observed by Autoprobe-PC (Park Scientific Instruments: PSI) in non-contact atomic force mode (NAFM) and magnetic force mode (MFM) with a cobalt coated cantilever (Co-Si_3N_4) which is commercially available. Before taking images, the cantilever was magnetized in z-direction (perpendicular to the cantilever and the sample), which coincides with the oscillation direction of the cantilever. Force constant of the cantilever was 0.05

N/m. Scan speed was 5 Hz. AFM and MFM images of the surface were recorded for the same region. The structure of the film was identified by an X-ray diffractometer (Rikagu D/MAX2400) with Cu-Kα radiation. Lattice constant was calculated by extrapolation of Nelson-Riley fitting: $\cos^2\theta/\sin\theta+\cos^2\theta/\theta$ *vs.* lattice constant. The pattern was compared with stoichiometric magnetite single crystal and pressed pellet. The Mössbauer (Fast Comtech.) spectrum was recorded at room temperature with Co^{57} source doped in metallic rhodium which was oscillated in a sinusoidal mode. The doppler velocity of spectra was calibrated with α-Fe foil (25 μm in thickness). Resistivity was measured by 4 probe or 2 probe dc method using a nanovoltmeter (Keithley 182) and a current source (Keithley 224) or an electrometer (Keithley 617). Temperature of the sample was controlled by a closed cycle helium refrigerator (APD HC-2) and a temperature controller (LakeShore M330).

Results and Discussion

AFM/MFM. Figure 2(a) is a NAFM image showing surface morphology of the LEP film. Representative size of the particle which exists in the surface of LEP film was about 0.2 μm in diameter. The size is close to that of the powder prepared by the supercritical fluid drying method.[11] Each particle is surrounded by other particles and top of a particle is cone-shaped as shown in Figure 2(b). Dark curved valley in Figure 2(b) is contact-boundary of particles. This morphology was confirmed by contact AFM and scanning electron microscopy (SEM). The morphology was very similar to the SEM picture of LEP ferrite film that was reported by Abe *et al.*[5]

According to the operation mechanism of MFM, height in MFM image depends on the magnetic interaction between the sample surface and the magnetized cantilever. Therefore we could understand submicromagnetic structure of surface of a sample by MFM. Figure 3 is a 3-D image of MFM. There is striking difference between Figure 2(b) and Figure 3, where both images are recorded for the same area. The valley region (black area) of the NAFM image appeared as high region (white area) in the MFM image. Flat region in the MFM image corresponds to the top region of a particle in NAFM (marked as A). These results indicate that contact boundary region of particles has attractive magnetic force due to magnetic poles associated with the surface termination of particles or magnetic domain.[10] In this region the attractive force between surface and cantilever was inversely proportional to the distance between them. But the other parts of the particle interact weak attractive or repulsive magnetic force against cantilever. One could see trace of patterns along the arrow in Figure 3. We think this pattern is magnetic domains which were found by other workers[10,30] on the surface of magnetite single crystal. The bumps in the front section of Figure 3 may be a part of the magnetic domains which result from the presence of free poles on the surface associated with oppositely magnetized domain. These results imply that the surface of LEP film consists of magnetic particles which are magnetically divided from the others. The XRD pattern of the LEP film matched well with that of magnetite without impurity peaks (Figure 4). Therefore, it is possible to assume that main composition of magnetically isolated particles on the LEP film is magnetite, as discussed in next sections.

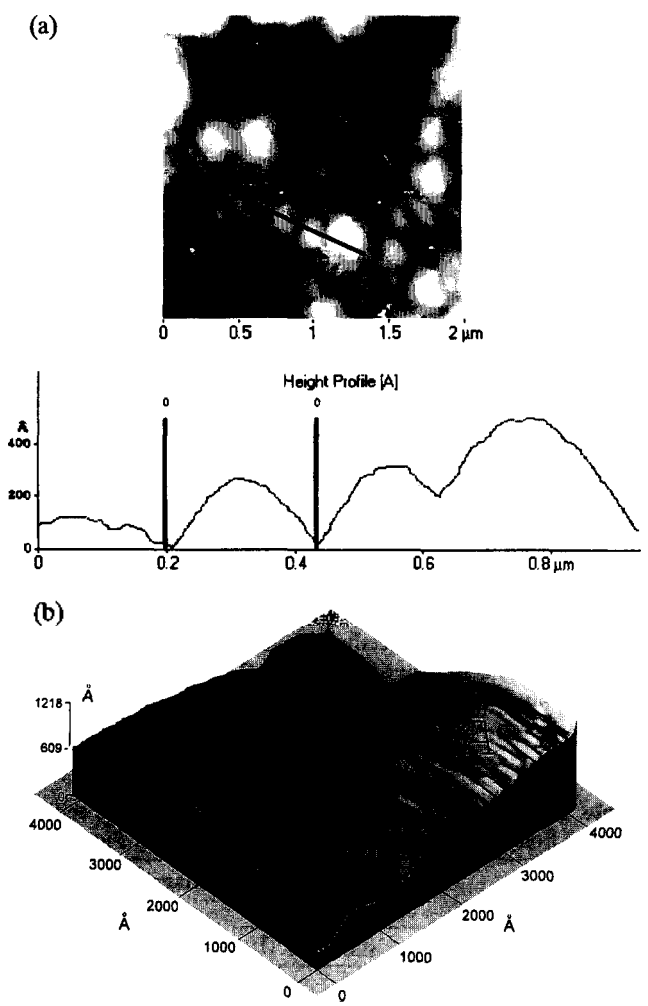

Figure 2. (a) Noncontact atomic force microscope (NAFM) image and hight profile of LEP film. (b) NAFM image of LEP film. The image is the other part of (a). Marked region (A) is cone-shaped.

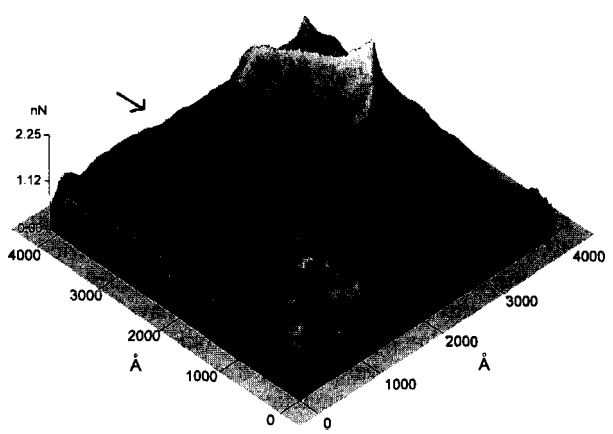

Figure 3. Magnetic force microscope (MFM) image of LEP film. The arrow indicates the presence of magnetic domain.

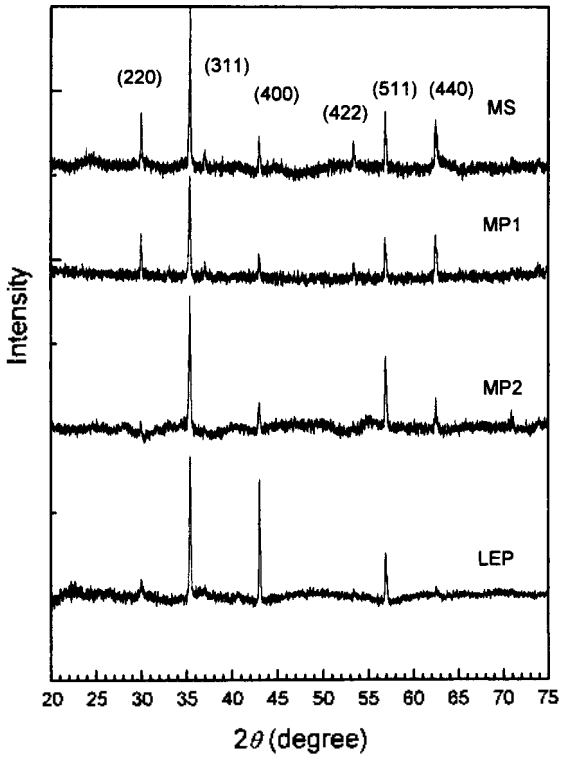

Figure 4. Powder X-ray diffraction patterns of MS, MP1, MP2 and LEP film.

XRD. The XRD pattern of the LEP film is shown in Figure 4. The pattern of LEP film was compared with those of synthetic magnetite single crystal (99.999% MS) and pressed pellets of magnetite powder (99.997% MP1, MP2). The MS and MP1 were annealed at 1473 °C under controlled oxygen fugacity (CO/CO_2 mixture gas) to attain stoichiometric magnetite (δ=0).[14,31] To keep the controlled composition, MP1 was dropped to liquid nitrogen (77 K) and MS dropped to copper block. MP2 was annealed to attain δ=0.01 with the same process of MP1, but under different oxygen fugacity. Outside layers of both samples were trimmed to remove uneven phases which were formed during quenching process. The single crystal and pellets were ground into powder to get the XRD pattern. XRD patterns of MS, MP1, MP2 and LEP film were matched well with JCPDS data[32] of magnetite as shown in Figure 4. Lattice parameters which was calculated by the extrapolation of Nelson-Riley fitting[33] were 0.8390 nm for LEP film, 0.8404 nm for MS, 0.8400 nm for MP1 and 0.8388 nm for MP2 (fitting error $\pm$0.0005 nm). Generally a_o decreases along with 3δ; in other words a_o reduced when Fe^{3+} ions are excess in the inverse spinel lattice.[12,13] As Tamaura *et al.* reported[12] we could roughly estimate nonstoichiometric value of magnetite from the calculated a_o. MP2 and LEP film will have more positive δ, MS and MP1 will have less positive δ. The larger δ value represents higher ratio of Fe^{3+}/Fe_{total}.

Mössbauer. It is well known that the Mössbauer spectrum of the magnetite is magnetically split[24,27,29] as shown in Figure 5. We assumed that the spectrum has Lorentzian line shapes with $I_1 : I_2 : I_3 = 3 : 2 : 1$ and $I_{7-j} = I_j$ (j=1, 2, 3) intensity ratio and $\Gamma_{7-j} = \Gamma_j$ (j=1, 2, 3) line widths for each individual

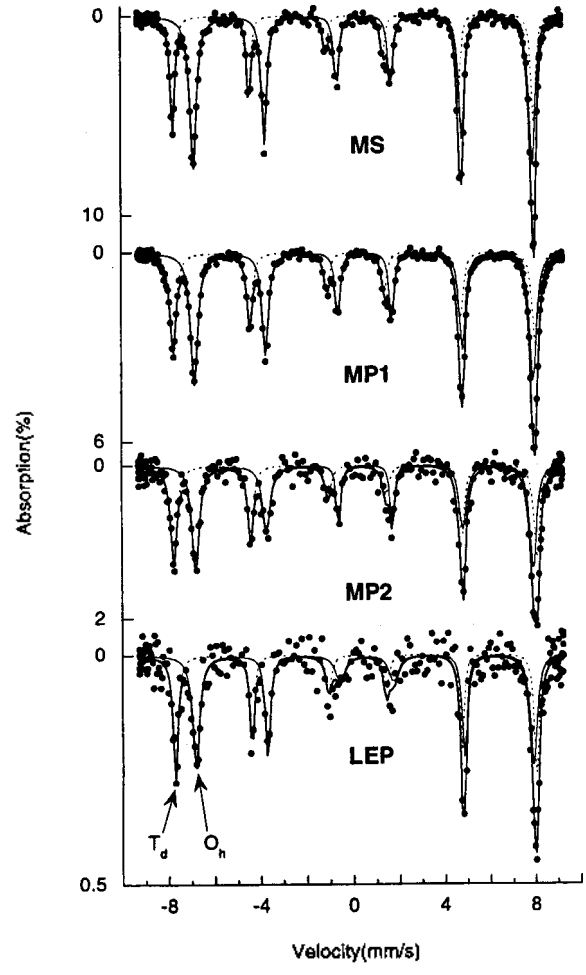

Figure 5. Mössbauer spectra of MS, MP1, MP2 and LEP film. The dotted and solid thin lines represent the fitting lines for Td and Oh sites, respectively.

six-line spectral pattern to analyze with a curve fitting program. The spectrum could be deconvoluted to two sextets marked by T_d, and O_h. The set of T_d results from tetrahedral sites (A site; Fe^{3+}) and the set of O_h results from octahedral sites (B site; Fe^{2+} and Fe^{3+}) of inverse spinel structure of magnetite. The chemical formula of stoichiometric magnetite is $(Fe^{3+})[Fe^{2+}Fe^{3+}]O_4$, where ( ) denotes tetrahedral site and [ ] denotes octahedral site. We will not use the general formula of magnetite ($Fe_{3(1-\delta)}O_4$) for a while to compare the site population of Fe ions. Table 1 is a list of the Mössbauer parameters. The area ratio (I_{Oh}/I_{Td}) of the peak

Table 1. Mössbauer parameters of the LEP film, MP, and MS, obtained from deconvolution of the spectra shown in Figure 5

Sample	I_{Oh}/I_{Td}	Isomer shift (mm/s)		Magnetic hyperfine field (kOe)	
		T_d (A) site	O_h (B)	T_d site	O_h site
MS	1.98	0.28	0.68	490	460
MP1	1.57	0.29	0.68	492	460
MP2	1.23	0.30	0.68	494	459
LEP	1.37	0.28	0.68	490	458
Error	0.05	0.01	0.01	2	2

corresponds to the number of Fe ions in octahedral sites divided by the number of Fe ions in tetrahedral sites. While the ratio of MS is 1.98 which is very close to ideal ratio (2.00) for the stoichiometric magnetite, the ratio for MP1, MP2 and LEP films are 1.58, 1.23 and 1.37, respectively. These values are much lower than the ideal ratio. But the other main Mössbauer parameters are nearly the same as those of MS and reported value of magnetite[28]: isomer shifts for A site and B site are 0.28 and 0.68 mm/s, and corresponding magnetic hyperfine fields are 490 and 460 kOe, respectively. This result indicates that some Fe^{3+} of B sites are not involved in the well known electron exchange process between $Fe^{2+} \leftrightarrow Fe^{3+}$ in B sites and these Fe^{3+} in B sites contribute to the sextet of T_d. The formation of this kind of Fe^{3+} in B sites was reported in ferrite solid solutions such as Fe_3O_4-γ-Fe_2O_3,[28] Ni-Fe_3O_4 systems[28] and epitaxial thin film of magnetite.[24,29] In these systems, sextet of T_d is due to the contribution of Fe^{3+} in both A and B sites, and sextet of O_h is due to the contribution of electron exchange between Fe^{2+} and Fe^{3+} in the B-sites, forming average valence nearly $Fe^{2.5+}$.[24,25,29] Therefore we could estimate the cation distribution of LEP film from the I_{Oh}/I_{Td} of LEP film, assuming that some of the Fe^{3+} in B sites are not included in the exchange process and contribute to sextet of T_d. The estimated formula for the LEP film is $(Fe^{3+}_{1.00})[Fe^{3+}_{0.27}Fe_{1.73}]O_4$. The valence of $Fe_{1.73}$ in B sites is +2.42 which is smaller than that of ideal magnetite (+2.50). The uncertainty in curve fitting process of Mössbauer spectra might cause the error in the estimated valence. These results indicate that LEP film consists of magnetite and special Fe^{3+} ions which do not take part in the electron exchange. By the same method we could estimate chemical formula for MP1 as $(Fe^{3+}_{1.00})[Fe^{3+}_{0.16}Fe_{1.84}]O_4$. The valence of $Fe_{1.84}$ is +2.45, and the number of Fe^{3+} in B sites is less than LEP film. The formula for MP2 will be also $(Fe^{3+}_{1.00})[Fe^{3+}_{0.35}Fe_{1.65}]O_4$, and the valence of $Fe_{1.65}$ is +2.39. Pycnometric (solvent CCl_4) density of the MP1 and MP2 was ~4.2 g/cm^3, which corresponds to 81% of that of magnetite (5.2 g/cm^3). The different density means that MP1 and MP2 have inner pores which could trap the annealing gas. The gas which was trapped at the pore might produce the special Fe^{3+} ions in the B sites during the quenching process. Because of large diffusion coefficient of oxygen in magnetite, outer surface of magnetite can be altered regardless of the quenching speed.[15] Therefore, the special Fe^{3+} ions will be localized near the pore. When we assume that valences of the $Fe_{1.73}$ in LEP film, $Fe_{1.84}$ in MP1 and $Fe_{1.65}$ in MP2 as +2.5, chemical formulas for LEP film, MP1 and MP2 can be written in general form as $Fe_{2.95}O_4$, $Fe_{2.97}O_4$ and $Fe_{2.94}O_4$, respectively.

Table 2. Chemical formulas which were estimated by Mössbauer spectra of the samples, nonstoichiometrys (δ) which were estimated by Verwey transition temperature, and lattice parameters (a_o)

Sample	Tv	Formula estimated by Mössbauer	δ from Tv	Lattice parameter (nm)
MS	~121	$(Fe^{3+})[Fe_2]O_4$	~0.00	0.8404
MP1	~121	$(Fe^{3+}_{1.00})[Fe^{3+}_{0.16}Fe_{1.84}]O_4$	~0.00	0.8400
MP2	~85	$(Fe^{3+}_{1.00})[Fe^{3+}_{0.35}Fe_{1.65}]O_4$	~0.01	0.8388
LEP	N/A	$(Fe^{3+}_{1.00})[Fe^{3+}_{0.27}Fe_{1.73}]O_4$	~N/A	0.8390

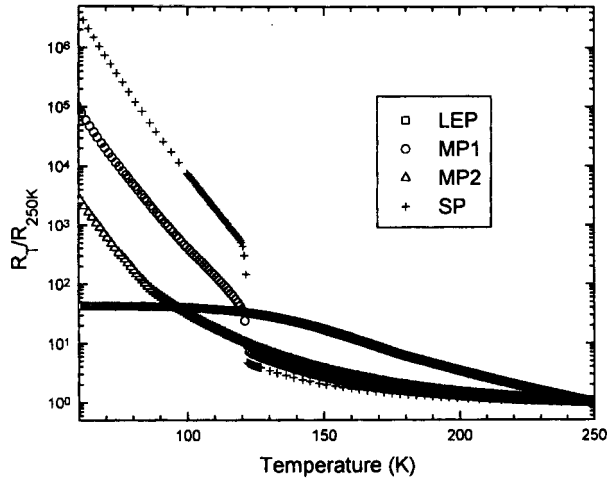

Figure 6. Temperature dependence of resistivity of MS, MP1, MP2 and LEP film. RT/R_{250K} is the resistance ratio at a temperature divided by resistance at 250 K.

The δ value of LEP film is between those of MP1 and MP2. Table 2 is a list of chemical formulas and some other physical parameters.

Resistivity. Figure 6 is the plots of temperature *vs.* R_T/R_{250K} for MS, MP1, MP2 and LEP film. MS and MP1 have a break around 121 K in the plot. This discontinuity in the plot is related to Verwey transition of magnetite.[15] We summarized Verwey transition temperatures of samples in Table 2. According to reports of Honig *et al.*,[14,15] the 3δ corresponding to Tv=121 K is close to zero. Therefore, both samples have stoichiometric magnetite phase. In Mössbauer experiment, however, MS and MP1 are different in Fe ion distribution. MS is close to ideal magnetite, but MP1 has special Fe^{3+} ions in B sites. Assuming that the special Fe^{3+} ions would be localized near the inner pore of MP1, electrical conduction properties of MP1 could be explained. The Fe^{3+} rich phase will not act as electron conduction path, but magnetite phase close to the ideal one will construct main conduction path in MP1. And if δ of the magnetite phase is close to zero, Tv of the MP1 will be ~121 K as shown in Figure 6. Therefore we conclude that MP1 has ideal magnetite phase which constructs the conduction path. The reduced resistivity jump width of MP1 at Tv may come from the presence of special Fe^{3+}. In general, more disordered magnetite has reduced resistivity below Tv and transition width at Tv,[14,17] as shown in Figure 6. Temperature dependence of resistance for MP2 is changed around 85 K in Figure 6. This change is related to Verwey transition. From the δ *vs.* Tv relationship,[14] we estimated nonstoichiometry of the conduction path in MP2: δ ~0.01. This is expected value from the annealing condition of MP2.[31] From the Mössbauer data and the resistivity data therefore, the special Fe^{3+} in B site of MP2 would be localized near the pores.

One can apply the same arguments to Tv of films.[34] LEP film does not show any Verwey transition within the experimental temperature range (12 K-300 K), even though LEP film is more stoichiometric than MP2. This indicates that nonstoichiometric value (3δ) of the magnetite phase which is electric conduction path of LEP film is larger than 0.039 in $Fe_{\gamma(1-\delta)}O_4$. This can be explained if we assume that

the special Fe^{3+} ions in LEP film are more evenly distributed all over the film than in MP2. If they are localized in particular sites, the film could have Verwey transition in the range of 85 K-121 K due to the more stoichiometric phase as MP2 had Tv. MP2 is more nonstoichiometric than LEP film but has Tv. Therefore, we could suggest that LEP film is more homogeneous than MP1 and MP2.

Temperature dependence of the resistance of LEP film is different from that of MPs and MS. From room temperature to around 120 K, the temperature dependence of LEP film is similar to highly doped magnetite single crystals.[35] This implies that the conduction mechanism of LEP film is very similar to highly doped magnetite in the temperature region. However, below the temperature region the resistance did not depend on the temperature. We do not have reasonable explanation for this behaviour, but it might be related with particle size or compactness of LEP film. Our ongoing SPM and ac susceptibility studies will reveal the actual ion distributions and conduction process in MPs and LEP film.[36]

Conclusions

We have compared some physical properties of LEP magnetite film which was deposited on a slide glass substrate from aqueous solutions of $FeCl_2$ and $NaNO_2$ at 90 °C with magnetites: single crystal (MS), and pressed pellets (MP1 and MP2). Lattice constant of the film was 0.8390 nm which is shorter than those of single crystalline magnetite (0.8406 nm) and JCPDS data (0.8396 nm). This indicates that the film is a nonstoichiometric magnetite. From the Mössbauer experiments we found that cation distribution of the film was $(Fe^{3+}_{1.00})[Fe^{3+}_{0.27}Fe_{1.73}]O_4$, where $Fe^{3+}_{0.27}$ did not take part in the exchange process between $Fe^{2+} \leftrightarrow Fe^{3+}$ in O_h sites. The formula corresponds to the $Fe_{2.95}O_4$. Because of large nonstoichiometric value (3δ=0.05), the film did not have Verwey transition in electrical conductivity measurement. However, MP2 ($Fe_{2.94}O_4$), 3δ=0.06, had Verwey transition at 85 K, due to more stoichiometric magnetite phase which constructs conduction path. Therefore, we could suggest that the film might be homogeneous than pressed pellets and highly nonstoichiometric magnetite phase. The suggested model could be confirmed by careful SPM research and ac susceptibility measurement. On the surface of the film, magnetite particles of about 0.2 μm in diameter were identified by NAFM and MFM. This is the first MFM study for the fine particles of LEP ferrite film.

Acknowledgment. We wish to thank Prof. J. M. Honig (Purdue Univ. Chem. Dept.) for useful conversations and P. A. Metcalf (Purdue Univ. Phys. Dept.) for her assistance in sample preparation. This work was supported by Korean Ministry of Education through Research Fund (BSRI-96-2455) and in part by Korea Science and Engineering Foundation (KOSEF-951-0303-032-2).

References

1. Abe, M.; Tamaura, Y. *Jpn. J. Appl. Phys.* **1983**, *22*, L 511.
2. Itoh, T.; Hori, S.; Abe, M.; Tamaura, Y. *IEEE Trans. Mag. Jpn.* **1991**, *6*, 214.
3. Abe, M.; Tanno, Y.; Tamaura, Y. *J. Appl. Phys.* **1985**, *57*, 3795.
4. Abe, M.; Itoh, T.; Tamaura, Y. *Thin Solid Films* **1992**, *216*, 155.
5. Abe, M.; Itoh, T.; Zhang, Q. *Trans. Mat. Res. Soc. Jpn.* **1994**, *15B*, 1117.
6. Zhang, Q.; Itoh, T.; Abe, M. *J. Appl. Phys.* **1994**, *75*, 7171.
7. Palacin, S.; Hidber, P. C.; Bourgoin, J.; Miramond, S.; Fermon, C.; Whitesides, G. M. *Chem. Mater.* **1996**, *8*, 1316.
8. Binnig, G.; Rohrer, H.; Gerberch, C.; Weibel, E. *Phys. Rev. Lett.* **1982**, *49*, 57.
9. Wiesendanger, R.; Shvets, I. V.; Burgler, D.; Tarrach, G.; Guntherodt, H. J.; Coey, J. M. D.; Graser, S. *Science* **1992**, *255*, 583.
10. Moloni, K.; Moskowitz, B. M.; Dahlberg, E. D. *Geophys. Res. Lett.* **1996**, *23*, 2854.
11. Yuan, C.; Yang, X.; Fu, D.; Lu, Z.; Liu, J.; Zhang, C.; Wu, T.; Wang, L.; Peng, S. *J. Solid State Chem.* **1996**, *121*, 492.
12. Tamaura, Y.; Tabata, M. *Nature* **1990**, *346*, 255.
13. Alekseyeva, I. P.; Voronin, D. V.; Goldberg, I. S. *Nefedova Dokl. Akad. Nauk SSR* **1987**, *296*, 1217.
14. Honig, J. M. *Proc. Indian Acad. Sci. (Chem. Sci.)* **1986**, *96*, 391.
15. Honig, J. M. *J. Alloy and Compounds* **1995**, *229*, 24.
16. Kim, D.; Honig, J. H. *Phys. Rev. B* **1994**, *49*, 4438.
17. Kozlowski, A.; Metcalf, P.; Kakol, Z.; Honig, J. M. *Phys. Rev. B* **1996**, *53*, 15113.
18. Kozlowski, A.; Kakol, Z.; Kim, D.; Zalecki, R.; Honig, J. M. *Phys. Rev. B* **1996**, *54*, 12093.
19. Kozlowski, A.; Kakol, Z.; Kim, D.; Zalecki, R.; Honig, J. M. *Z. Anorg. All. Chem.* **1997**, *623*, 115.
20. Kim, D.; Cho, J. W. *J. Kor. Chem. Soc.* **1997**, *41*, 271.
21. (a) Kim, D. KOSEF report (1997). (b) Park, J. C.; Kim, D. manuscript in preparation.
22. Chen, Q. W.; Qian, Y. T.; Chen, Z. Y.; Xie Y.; Zhou, G. E.; Zhang, Y. H. *Mat. Lett.* **1995**, *24*, 85.
23. Kleint, C. A.; Semmelhack, H. C.; Lorenz, M.; Krause, M. K. *J. Mag. Mag. Mat.* **1995**, *140-144*, 725.
24. Voogt, F. C.; Fujii, T.; Hibma, T.; Hoefman, M.; Smulders, P. J. M.; Wijnja, G. H.; Zhang, G. L.; Nisesen, L. *Hyperfine Interaction* **1996**, *97/98*, 99.
25. Lee, J. S.; Itoh, T.; Abe, M. *J. Kor. Phy. Soc.* **1995**, *28*, 375.
26. Iwasaki, I.; Katsura, T.; Ozawa, T.; Yoshida, M.; Mashima, M.; Haramura, H.; Iwasaki, B. *Bull. volc. Soc. Jpn. Ser. II* **1960**, *5*, 9.
27. Haley, G.; Mullen, J. G.; Honig, J. M. *Solid State Comm.* **1989**, *6*, 285.
28. Kodama, T.; Tabata, M.; Sano, T.; Tsuji, M.; Tamaura, Y. *J. Solid State Chem.* **1995**, *120*, 64.
29. Voogt, F. C.; Hibma, T.; Zhang, G. L.; Hoefman, M.; Niesen, L. *Surface Sci.* **1995**, *331-333*, 1508.
30. Proksch, R.; Foss, S.; Orme, C.; Sahu, S.; Moskowitz, B. *J. Appl. Phys.* **1994**, *75*, 689.
31. (a) Dieckman, R. *Ber. Bunsenges. Phys. Chem.* **1982**, *86*, 112. (b) Dieckman, R.; Schmalzried, H. *ibid* **1977**, *811*, 344. (c) Shepherd, J. P.; Sandberg, C. *J. Rev. Sci. Instrum.* **1984**, *55*, 1696. (d) Harrison, H. R.; Aragon,

R. *Mat. Res. Bull.* **1978**, *13*, 1097.
32. (a) JCPDS (Joint Committee on Powder Diffraction Standards) data base 19-629. (b) Cornell, R. M.; Schwertmann, U. *The Iron Oxides*; VCH: Weinheim, Germany, 1996, p 167.
33. Azaroff, L. B. *The Powder Method*; McGraw Hill: New York, N.Y. 1958, p 238.
34. Kleint, C. A.; Semmelhack, H. C.; Lorenz, M.; Krause, M. K. *J. Mag. Mag. Mat.* **1995**, *140-144*, 725.
35. Wang, P.; Kakol, Z.; Wittenauer, M.; Honig, J. M. *Phys. Rev. B* **1992**, *46*, 1975.
36. We found that ac susceptibility of magnetite suddenly changed at Tv. High sensitivity of ac susceptometer ($\sim 10^{-8}$ emu/g) could detect small amount of different stoichiometry of magnetite phase in LEP film.

A Theoretical Study on Vibrational Predissociation Rates of Ne-I_2

Jeonghee Seong and Hosung Sun

Department of Chemistry, Sungkyunkwan University, Suwon 440-746, and Center for Molecular Science, KAIST, Taejon 305-701, Korea
Received November 26, 1997

A new theoretical method, named the SCF-DWB-IOS approximation, is suggested to investigate the vibrational predissociation of triatomic van der Waals complexes. The meta stable vibrational excited states are described with SCF (self-consistent-field) approximation and the fragmented diatomic continuum states are determined by using IOS (infinite order sudden) approximation. The dissociation process itself is studied by using DWB (distorted wave Born) approximation. As a test case, the predissociation rates, rotational state distributions of products, and the lifetimes of vibrationally excited states of Ne-I_2 are all computed which are in reasonable agreements with other theoretical and/or experimental results. The suggested SCF-DWB-IOS approximation scheme is found to be a very simple but efficient theoretical tool to investigate the vibrational predissociation dynamics of small van der Waals complexes.

Introduction

The predissociation dynamics of van der Waals complexes has attracted a lot of attention both experimentally and theoretically.[1-30] In weakly bound molecules, vibrational motions deviate from harmonic behavior a lot even in the vibrational ground state. It is thus important to obtain the vibrational energy level structure of the complexes from potential energy functions and to theoretically investigate vibrational predissociation process of van der Waals complexes. The need for theoretical methods arises from a rapid progress in experimental van der Waals complex spectroscopy.

For triatomic van der Waals complexes, many theoretical and experimental studies have been made to understand the dissociation dynamics.[23,24] The vibrational predissociation process, in which excess vibrational energy flows into a weak van der Waals bond to break it up, is particulary well studied. From a theoretical point of view, triatomic van der Waals complexes provide ideal model systems for the predissociation study. Because the electronic states involved are well studied, and the potential energy surfaces are known, and the relevant quantities like transition dipole moments are well characterized.

We propose a new approximate quantum mechanical method which can describe the vibrational predissociation dynamics of triatomic van der Waals complexes, *e.g.*, particulary diatom-rare gas atom complexes. This new method is designed to calculate dissociation rates, lifetimes of metastable vibrational excited states and rotational state distribution of dissociated diatomic fragments.

To determine vibrational excited states of triatom complexes (bound state), we utilize a self-consistent-field (SCF) approximation. The SCF approximation and the configuration interaction (CI) method are used to calculate the vibrational energy levels of triatomic van der Waals complex. The SCF and CI method are widely used in electronic structure calculations, but the vibrational structure calculations using SCF and CI are not frequently reported.[27,31] In SCF method,[1,5,20,21,22] the each vibrational mode is described as moving in an effective field, being the average of the full potential over the motions of all the other modes, and consists of wavefunctions called modal wavefunctions corresponding to orbitals in electronic structure theory. The validity and accuracy of the SCF approximation which omits the correlation between modes depend on the choice of coordinates, because each modal wavefunction is represented with each variable composing the coordinates chosen. The correlation part missing in SCF approximation is incorporated in CI method. In CI, the true vibrational wavefunctions are expressed in linear combination of configurations which are a product of modal wavefunctions. And the CI matrix is set up and diagonalized to have more exact vibrational energies and wavefunctions. In the previous report,[27] the comparison of SCF with CI is made to find that the simple SCF is a very reasonable method when Jacobi